

NiAu: A testing ground for theories of phase stability

C. Wolverton and Alex Zunger

National Renewable Energy Laboratory, Golden, CO 80401

(January 20, 2022)

Abstract

The theory of phase stability in the NiAu alloy system is a popular topic due to the large size mismatch between Ni and Au, which makes the effects of atomic relaxation critical, and also the fact that NiAu exhibits a phase separation tendency at low temperatures, but measurements at high-temperature show an ordering-type short-range order. We have clarified the wide disparity which exists in the previously calculated values of mixing energies and thermodynamic properties by computing "state-of-the-art" energetics (full-potential, fully-relaxed LDA total energies) combined with "state-of-the-art" statistics (k-space cluster expansion with Monte Carlo simulations) for the NiAu system. We find: (i) LDA provides accurate mixing energies of disordered Ni_xAu_x alloys ($H_{\text{mix}} < +100$ meV/atom) provided that both atomic relaxation (a 100 meV/atom effect) and short-range order (25 meV/atom) are taken into account properly. (ii) Previous studies using empirical potentials or approximated LDA methods often underestimate the formation energy of ordered compounds, and hence also underestimate the mixing energy of random alloys. (iii) Measured values of the total entropy of mixing combined with calculated values of the configurational entropy demonstrate that the non-configurational entropy in NiAu is large, and leads to a significant reduction in miscibility gap temperature. (iv) The calculated short-range order agrees well with measurements, and both predict ordering in the

disordered phase. (v) Consequently, using inverse Monte Carlo to extract interaction energies from the measured/calculated short-range order in NiAu would result in interactions which would produce ordering-type mixing energies, in contradiction with both experimental measurements and precise LDA calculations.

I. INTRODUCTION

The NiAu alloy system is physically interesting because, on one hand it exhibits a phase separation tendency at low temperatures and positive mixing enthalpies [1] and, on the other hand, an ordering-type short-range order (SRO) at high temperatures. [2] Also, the fcc Ni and Au constituents possess a large lattice mismatch ($a_{\text{Au}} - a_{\text{Ni}} \approx 15\%$), thus making this system a critical test for any alloy phase stability theory hoping to capture the effects of atomic relaxation. Important early experimental and theoretical work on this alloy includes the work of Moss et al. [3,4], Cohen et al. [5,2,6], and Cook and de Fontaine [7]. The coexistence of phase separation (at low T) with short-range ordering (at high T) in the same alloy system might have been naively construed to imply a change from repulsive ("ferromagnetic") interactions at low T to attractive ("anti-ferromagnetic") interactions at higher T . The change would have been surprising, given that no electronic, magnetic, or structural change is observed in this temperature range. The answer to this puzzle was given by Lu and Zunger: [8] The excess energy for a disordered $\text{Ni}_x\text{Au}_{1-x}$ alloy or an ordered compound of type $\text{Ni}_x\text{Au}_{1-x}$ is given by:

$$H = E(a_{\text{eq}}) - [(1-x)E_{\text{Ni}}(a_{\text{eq}}^{\text{Ni}}) + xE_{\text{Au}}(a_{\text{eq}}^{\text{Au}})]; \quad (1)$$

and may be written [9] $H = H_{\text{SRO}} + E_{\text{VD}}$, where H_{SRO} is the constant-volume, "spin- $\uparrow\downarrow$ " energy required to create $\text{Ni}_x\text{Au}_{1-x}$ out of Ni and Au, each already prepared at the alloy lattice constant a_{eq} , and E_{VD} is the volume deformation energy required to hydrostatically deform Ni and Au from their respective $a_{\text{eq}}^{\text{Ni}}$ and $a_{\text{eq}}^{\text{Au}}$ to a_{eq} . In Ref. [8], it is demonstrated that SRO is determined by the constant volume energy change H_{SRO} , which is negative (ordering, or "anti-ferromagnetic") in NiAu, indicating an ordering tendency of SRO. However, $E_{\text{VD}} - G(x)$ is large and positive, making $H > 0$. And, since long-range order is determined by H , NiAu shows phase-separating ("ferromagnetic") long-range order. This analysis leads to two unexpected conclusions: First, that the time-honored Ising-like representation of alloy thermodynamics which includes only "spin- $\uparrow\downarrow$ " energies of the H_{SRO} type,

but ignores the elastic energy $G(x)$ will fail in explaining basic stability trends for systems such as NiAu. Second, since measurements or calculations of the SRO are insensitive to physical effects (i.e., elastic deformation E_{VD}) that control measurements/calculations of mixing enthalpies H , the often-used practice [10] of "inverting" the SRO profile to extract interaction energies that are then used to predict mixing enthalpies is fundamentally flawed. Specifically, inversion of the SRO of NiAu will produce ordering-like interaction energies which, when used to calculate mixing enthalpies will produce (ordering-like) negative values, while the measured ones are strongly positive. [1,11]

For these and other reasons, the theory of phase stability in NiAu has recently become quite popular [8,12,16,13{15,19,18,17] (Table I). These calculations are distinguished by the methods used for (i) energetics ($T = 0$ K) and (ii) statistics ($T \neq 0$). Energy calculations ($T = 0$ K) for this system have been performed by a wide variety of techniques: First-principles calculations, both full-potential (FLAPW [8] and FLMT0 [12]) and atomicsphere-approximation (LMTO [13{15] and ASW [16]), as well as semi-empirical (EAM [17]) and empirical potentials [18,12,19]. There are significant variations in the computed energetics (Table I). Statistics have been applied to these calculations using cluster expansions (CE) such as $-G$ [9], Connolly-Williams [20], and second-order expansions. [21]

The purpose of this paper is thus three-fold:

First, we would like to clarify the conflicting energetic and statistical results (Table I) by computing "state-of-the-art" energetics for NiAu alloys (full-potential LAPW total energies including full atomic relaxation) combined with "state-of-the-art" statistics (a k -space CE [33] with Monte Carlo simulations). These computations will clarify whether the better agreement with experimental H obtained by approximated methods (e.g., empirical and semi-empirical potentials, as well as atomicsphere-approximation methods) relative to full LDA methods is fundamental or accidental.

Second, we would like to address the issue of why the calculated miscibility gap temperatures are often much too high compared with the experimentally assessed phase diagram [1]. In Table I, one can see a fixed ratio between calculated miscibility gap temperatures T_{MG}

and the calculated H_{mix} . In fact, all previous calculations (except the EAM calculations of Asta and Foiles [17]) very nearly follow the ratio obtained using mean-field configurational entropy: $k_B T_{MG} = H_{mix} = 2$. However, the experimental value of this ratio is 1.2. We will examine this apparent discrepancy between experimental H_{mix} and T_{MG} below.

Third, we would like to examine the SRO in NiAu and discuss the implications of this SRO on "inverse" techniques, mentioned above, for calculating phase stability in alloys. We will offer a challenge to practitioners of the inverse Monte Carlo method.

II. CHECKING ORDERED COMPOUND FORMATION ENERGIES

Table I summarizes the previous calculations on the mixing enthalpies of random NiAu alloys. The wide discrepancy between calculated values of H_{mix} (48-170 meV/atom) is apparent from this table. Since mixing enthalpies H_{mix} of random alloys can be expressed [see, e.g., Eq. (3b) in Ref. [22]] as a linear combination of formation enthalpies $H_f(\cdot)$ of certain ordered compounds f, g , the discrepancies in H_{mix} must reflect discrepancies in $H_f(\cdot)$. But formation enthalpies of small-unit-cell ordered compounds can be computed accurately and reliably via full-potential fully-relaxed LDA methods. Our strategy will thus be to trace the source of the discrepancy in H_{mix} to the values of formation energies of various NiAu_q ordered compounds, as shown in Table II. Examining this table leads to several interesting points regarding the energetics in NiAu:

A. FLMT vs. ASA methods (LMT, ASW)

In comparing the full-potential LMT [12] to LMT-ASA [15] calculations, one can see significant and strongly configuration-dependent discrepancies, even when considering unrelaxed configurations. For example, the Z2 structure [a NiAu₂ (001) superlattice] has an unrelaxed formation energy which is nearly 100 meV/atom lower in the LMT-ASA calculation than in the full-potential LMT one. Thus, the ASA-based calculations (LMT,

ASW) in the NiAu system cannot be trusted for the kind of quantitative energetics required in phase stability studies. [23]

B. Harmonic vs. anharmonic relaxation

In a large lattice-mismatched system like NiAu, the effects of atomic relaxation are likely to be crucial. Although straightforward, fully relaxing all of the cell-internal and cell-external degrees of freedom can be computer intensive. One alternative to full atomic relaxation (using quantum mechanical forces and total energy minimization) which has been used in NiAu [8] is to use continuum elasticity theory [24] to find the relaxed geometry, with a subsequent LDA calculation with this geometry to find the relaxed energetics. Continuum elasticity theory can be used as a relaxation model by realizing that many ordering NiAu_q compounds can be described as "superlattices" along some special orientations \hat{k} . Continuum elasticity then provides the equilibrium interlayer spacing c_{eq} along \hat{k} as a function of the externally-fixed perpendicular lattice constant a_\perp as the minimum of the epitaxial strain energy due to the external constraint:

$$c_{eq}(\hat{k}; a_\perp) = a_{eq}^{(0)} + [2 - 3q^{(0)}(a_\perp; \hat{k})] a_{eq}^{(0)} a_\perp + \dots \quad (2)$$

$$q(a_\perp; \hat{k}) = \frac{E_{epi}^{eq}(a_\perp; \hat{k})}{E_{bulk}(a_\perp)} \quad (3)$$

where $E_{eq}^{(0)}$ and $a_{eq}^{(0)}$ are the equilibrium energy and lattice constant of the cubic material. E_{epi}^{eq} is the energy of the alloy constituent subject to the biaxial constraint that the lattice constant perpendicular to \hat{k} is externally fixed to be a_\perp . $E_{bulk}(a_\perp)$ is simply the deformation energy change upon hydrostatically distorting the material from a_{eq} to a_\perp . The central quantity in these elastic calculations is the "strain reduction factor" $q(a_\perp; \hat{k})$. In continuum elasticity theories, $q(a_\perp; \hat{k})$ is given by

$$q(a_\perp; \hat{k}) = 1 - B = [C_{11} + (a_\perp; \hat{k})] : \quad (4)$$

where

$$= C_{44} - (C_{11} - C_{12})/2 \quad (5)$$

is the elastic anisotropy, $B = (C_{11} + 2C_{12})/3$ is the bulk modulus, and C_{ij} are elastic constants. In the harmonic approximation, $q(a_2; \hat{k})$ is further assumed to be a_2 -independent, and $\chi_{\text{ham}}(\hat{k})$ is the following geometric function for the direction $\hat{k} = (l; m; n)$:

$$\begin{aligned} \chi_{\text{ham}}(l; m; n) &= \frac{4(l^2m^2 + m^2n^2 + n^2l^2)}{(l^2 + m^2 + n^2)^2} \\ &= \frac{4}{5} \left[\frac{1}{4} [K_0(l; m; n) - \frac{2}{21} K_4(l; m; n)] \right] \end{aligned} \quad (6)$$

where K_L are the Kubic harmonics of angular momentum L .

Using Eqs. (2)–(6) thus provides predicted relaxed geometries $c_{\text{eq}}(\hat{k}; a_2)$ for alloy compounds (e.g., the Z2 structure) given the elastic constants and $a_{\text{eq}}^{()}$. Indeed, these equations have been routinely used (see review in Ref. [25]) to predict the distortion $c_{\text{eq}} - a_{\text{eq}}$ of In_2S_3 grown epitaxially on a substrate with lateral lattice constant a_2 . Comparison to LDA calculations [26] shows that for semiconductors with lattice mismatch $(a_{\text{eq}} - a_2)/a_2 < 7\%$, the harmonic expressions (4)–(6) work very well down to a monolayer thickness. However, we find that for noble- and transition-metal alloys with a much larger lattice mismatch (e.g., NiAu, CuAu with $a_{\text{eq}}/a_2 = 15\%, 12\%$, respectively), anharmonic corrections are important. As we will see below in Sec. III C, this is manifested by the fact that $q(a_2; \hat{k})$ of Eq. (4) now has additional terms to those appearing in the harmonic form of Eq. (6). These anharmonic terms in $q(a_2; \hat{k})$ lead via Eq. (4) to corrections to $q(a_2; \hat{k})$, and consequently via Eq. (2) to the relaxation of the lattice constant $c_{\text{eq}}(\hat{k})$. Indeed, using the same FLAPW as Ref. [8], but minimizing the total energy quantum mechanically ("Fully relaxed" in Table II) rather than via the harmonic expression of Eq. (4) ("Partially relaxed" in Table II), we find a lower-energy relaxation for Z2: The LDA energy minimization gives $E(\text{Z2}) = -70.2 \text{ meV/atom}$, while LDA with harmonic relaxation gives -124.3 . For other structures, the effect is much lower. Nevertheless, anharmonic relaxation in NiAu alloys is large and cannot be neglected.

C. Empirical methods: Getting the right $H_{mix}(x;T)$ for the wrong reason?

We see from Table I that the methods that use empirical evaluations of $H_{mix}(l=2;1)$ [15,19,18,12,17] produce results that are lower, and thus closer to the measured $H_{mix}(l=2;1150)$ than methods that use converged, full-potential, fully relaxed approaches (i.e., the present work and Refs. [8,12]). Since there is a proportionality between H_{mix} and $H_f()$, we thus surmise that the empirical methods will produce formation energies $H_f()$ of ordered compounds that are lower than the LDA results for such systems. Indeed, Table II shows the formation energies of two of the empirical potential methods. By comparing these numbers to full-potential LDA energies, one can see that the empirical potentials systematically underestimate the formation energies of ordered compounds. Since the LDA method is expected to reproduce formation enthalpies of small-unit-cell ordered structures rather accurately, and since FLAPW gives a precise representation of the LDA, we think that the underestimation of FLAPW energies by the empirical methods is a rather serious limitation of these methods. The EAM of Ref. [17] was fit to the unrelaxed FLAPW calculations of Ref. [8], and thus reproduces these energies fairly well (except for the Z2 structure). However, the EAM severely overestimates the energetic effect of relaxation, and hence produces relaxed formation energies which are much lower than LDA, and in some cases are even negative. [27] It would be desirable to see more formation energies of ordered compounds from the empirical methods to determine the expectation of underestimation of $H_f()$ relative to LDA.

In summary, the reason that empirical methods agree with measured random-alloy mixing enthalpy better than LDA methods do is a systematic underestimation by the empirical methods of even the ordered compound energies.

III. PRESENT CALCULATIONS - FLAPW WITH K-SPACE CLUSTER EXPANSION

We have performed first-principles full-potential LAPW [28] calculations for pure Ni, pure Au, and a large number (31) of fcc-based Ni-Au compounds in order to construct an accurate cluster expansion. The total energy of each compound is fully minimized with respect to volume, cell-internal, and cell-external [29] coordinates using quantum-mechanical forces. We have used the exchange correlation of Wigner [30]. The muffin-tin radii are chosen to be 2.2 a.u. for Ni and 2.4 a.u. for Au. Brillouin-zone integrations are performed using the equivalent k-point sampling method, [31] with the k-points for each compound all mapping into the same 60 special k-points for the fcc structure. This mapping guarantees that the total energy per atom of an elemental metal calculated either with the fcc unit cell or with a lower symmetry (e.g., any of the compounds) are identical. All calculations performed are non-magnetic. (The spin polarization energy difference between ferro- and non-magnetic fcc Ni was calculated and found to be -50 meV/atom.)

The 31 calculated LAPW formation energies are given in Table III. Both relaxed and unrelaxed (total energy minimized with respect to volume, but with cell-internal and cell-external coordinates held fixed at ideal fcc positions) formation energies are shown. The nomenclature of the compounds studied is the same as given in [22]. Many of the compounds considered can be described as Ni_pAu_q "superlattices" along a particular orientation \hat{k} :

$$\begin{aligned}
 \text{Ni}_1\text{Au}_1 &: [100]; [111]; \\
 \text{Ni}_2\text{Au}_1 &: [100]; [011]; [111]; \\
 \text{Ni}_1\text{Au}_2 &: [100]; [011]; [111]; \\
 \text{Ni}_3\text{Au}_1 &: [100]; [011]; [201]; [111]; [311]; \\
 \text{Ni}_1\text{Au}_3 &: [100]; [011]; [201]; [111]; [311]; \\
 \text{Ni}_2\text{Au}_2 &: [100]; [011]; [201]; [111]; [311]; \\
 \text{Ni}_3\text{Au}_3 &: [100]; \\
 \text{Ni}_2\text{Au}_3 &: [100]:
 \end{aligned} \tag{7}$$

We also calculated the energies of six other structures: $L1_2$ (Ni_3Au and NiAu_3), $D7$ (Ni_7Au and NiAu_7), and two 8-atom "special quasi-random structures" [32], SQS14_a (Ni_6Au_2 and Ni_2Au_6). In addition the Ni_pAu_q long-period superlattice limits ($p; q \rightarrow 1$) needed in the construction of the k -space cluster expansion (see below) were computed for six principle directions: $[100]$, $[011]$, $[201]$, $[111]$, $[311]$, and $[221]$. The numerical error of the LAPW calculations of H_f is estimated to be ~ 10 meV/atom or less.

B. k -space cluster expansion

The NiAu formation energies H for structures are then mapped onto a cluster expansion using the k -space formulation of Laks et al. [33] Rather than a cluster expansion of H , we will expand with respect to a reference energy:

$$E_{\text{CE}}(\sigma) = H^{\text{LDA}}(\sigma) - E_{\text{ref}} \quad (8)$$

We will separate the CE into two parts: (i) the terms corresponding to pair interactions with arbitrary separation will be conveniently summed using the reciprocal-space concentration-wave formalism, and (ii) all terms but the pairs will be cast in real-space:

$$E_{\text{CE}}(\sigma) = \sum_k J(k) S(k; \sigma) + \sum_f D_f J_f \overline{\sigma}_f(\sigma); \quad (9)$$

The first summation includes all pair figures and the second summation includes only non-pair figures. In the reciprocal-space summation in Eq. (9), $J(k)$ and $S(k; \sigma)$ are the lattice Fourier transforms of the real-space pair interactions and spin-occupation variables, J_{ij} and \hat{S}_i , respectively, and the spin-occupation variables take the value $\hat{S}_i = \pm 1$ ($+1$) if the atom at site i is Ni (Au). The function $J(k)$ is required to be a smooth function by minimizing the integral of the gradient of $J(k)$. The real-space summation of Eq. (9) is over f , the symmetry-distinct non-pair figures (points, triplets, etc.), D_f is the number of figures per lattice site, J_f is the Ising-like interaction for the figure f , and $\overline{\sigma}_f$ is a product of the variables \hat{S}_i over all sites of the figure f , averaged over all symmetry equivalent figures of lattice sites.

The reference energy of Eq. (8) is chosen to contain in finite-range real-space elastic interaction terms. Subtracting these long-range terms from H^{LDA} before cluster expanding removes the $k \rightarrow 0$ singularity, and thus significantly enhances the convergence of the CE. [33] The form used for E_{ref} is

$$E_{\text{ref}} = \frac{1}{4x(1-x)} \sum_k E_{\text{CS}}^{\text{eq}}(\hat{k}; x) \mathcal{J}(k; x)^2 \quad (10)$$

where $E_{\text{CS}}^{\text{eq}}(\hat{k}; x)$ is the equilibrium constituent strain energy, defined as the energy change when the bulk solids Ni and Au are deformed from their equilibrium cubic lattice constants a_{Ni} and a_{Au} to a common lattice constant $a_?$ in the direction perpendicular to \hat{k} . $E_{\text{CS}}^{\text{eq}}(\hat{k}; x)$ can thus be written as the minimum of the following expression with respect to $a_?$:

$$E_{\text{CS}}^{\text{eq}}(\hat{k}; x) = (1-x)q^{\text{Ni}}(a_?; \hat{k}) E_{\text{bulk}}^{\text{Ni}}(a_?) + xq^{\text{Au}}(a_?; \hat{k}) E_{\text{bulk}}^{\text{Au}}(a_?): \quad (11)$$

where $q^{(\cdot)}(a_?; \hat{k})$ is given by Eq. (2).

The final expression used for the formation energy of any configuration is then

$$\begin{aligned} H(\cdot) = & \sum_k J(k) \mathcal{J}(k; x)^2 + \sum_f D_f J_f \overline{\mathcal{J}}_f(\cdot) \\ & + \frac{1}{4x(1-x)} \sum_k E_{\text{CS}}^{\text{eq}}(\hat{k}; x) \mathcal{J}(k; x)^2 \end{aligned} \quad (12)$$

The following input is needed to construct this Hamiltonian for Ni-Au: (i) the formation energies of a set of ordered fcc-based compounds (required to fit the values of $J(k)$ and J_f), and (ii) the epitaxial energies of fcc Ni and fcc Au (required to compute the anharmonic values of $E_{\text{CS}}^{\text{eq}}(\hat{k}; x)$). The output is a Hamiltonian [Eq. (12)] which (i) predicts the energy of any fcc-based configuration (i.e., not only ordered compounds) even 1000-atom cells or larger, (ii) possesses the accuracy of fully-relaxed, full-potential LDA energetics, and (iii) is sufficiently simple to evaluate that it can be used in Monte Carlo simulations, and thereby extend LDA accuracy to finite temperatures.

Laks et al. [33] demonstrated that the calculation of $E_{CS}^{eq}(\hat{k};x)$ of Eq. (11) is significantly simplified if one uses harmonic continuum elasticity theory [i.e., insert Eqs. (4)–(6) into Eq. (11)]; However, we have already seen evidence of anharmonic elastic effects in Ni-Au. Thus, we have performed LDA calculations of $q(a_2; \hat{k})$ directly from its definition in Eq. (2), rather than using the harmonic approximation in Eq. (6). In Fig. 1, we show the results of the LAPW calculations of $q^{Ni}(a_2; \hat{k})$ and $q^{Au}(a_2; \hat{k})$ for six principle directions: (100), (111), (110), (201), (311), and (221). It is clear that the calculated values of q are not independent of a_2 , but rather show a marked and non-trivial dependence on the perpendicular lattice constant. Thus, the lattice mismatch in Ni-Au appears to be too large for a harmonic continuum model of elasticity to be accurate. In particular, the value of $q^{Ni}(a_2; 100)$ is quite low upon expansion, indicating that Ni is elastically extremely soft in this direction. Au, on the other hand, becomes softest in the (201) direction for significant compression. In a separate publication, [34] we will demonstrate that the anharmonic effects can be cast analytically in terms of the harmonic expressions of Eqs. (4)–(6) by extending the expansion of \hat{k} :

$$(a_2; \hat{k}) = \sum_L a_L(a_2) K_L(\hat{k}) \quad (13)$$

to include angular momenta $L=6,8$, and 10 with the coefficients $a_L(a_2)$ obtained from LDA calculations rather than the $L=0,4$ expression of Eq. (6) used before. [33]

The results for $q^{Ni}(a_2; \hat{k})$ and $q^{Au}(a_2; \hat{k})$ are used to numerically minimize Eq. (11) and hence to find $E_{CS}^{eq}(\hat{k};x)$. The results for the CS energies are shown in Fig. 2. Here, also, the anharmonic effects are seen quite strongly as $E_{CS}^{eq}(\hat{k};x)$ for some directions cross with other directions and asymmetries of the various directions are not all the same (effects which could not occur in the harmonic model). The most prominent feature of $E_{CS}^{eq}(\hat{k};x)$ is that (100) is the softest elastic direction, which stems from the elastic softness of Ni along this direction. Ni being soft and Au being relatively hard along (100) leads to Ni(Au) being

highly distorted (nearly undistorted) for long-period (100) Ni-Au superlattices, and also leads to the marked asymmetry in $E_{CS}^{eq}(100;\mathbf{x})$ towards the Ni-rich compositions. Similar arguments can be applied to explain the opposite asymmetry of the (201) strain.

For E_{ref} to be useful in the k -space CE, one must be able to know this energy for all directions, not merely the ones for which it was calculated. To obtain such a useful form, we fit the constituent strain results of Fig. 2 to a series of Kubic harmonics (0-10th order) consistent with cubic symmetry ($L = 0,4,6,8,10$). This procedure provides not only a good fit of the calculated strain data, but also an analytic form to obtain the values of $E_{CS}^{eq}(\hat{\mathbf{k}};\mathbf{x})$ for all directions.

D. Stability of the cluster expansion

Using the calculated formation energies fH_f (Table III) and the anharmonic CS strain energy (Fig. 2), we then fit the coefficients $J(\mathbf{k})$ and fJ_f of the k -space CE using Eq. (9). We used all 33 calculated structures in the fit of the expansion, which included 20 pair, 5 triplet, and 3 quadruplet interactions. The standard deviation of the fitted energies relative to their LAPW values is 5.3 meV/atom, which is the same order of magnitude as the numerical uncertainties in LAPW. The results for pair and multibody interactions are shown in Fig. 3.

In order for the expansion to have a useful predictive capability, tests must be performed to assess the stability of the fit:

Changing the number of interactions: We performed tests of the stability of the fit with respect to the number of pair interactions, $N_{pairs} = (1 - 50)$. Figure 4 shows the standard deviation of the fit as a function of the number of pairs interactions included. It is clear that the fit is well converged for $N_{pairs} = 20$. We also tested the stability of the fit with respect to inclusion of more multibody interactions than are shown in Fig. 3: Including three additional triplet figures in the fit resulted in no change of the standard deviation of the fit, the added interactions had values < 2 meV/atom, and the original interactions

were changed by less than 2 meV/atom. Thus, the fit is stable with respect to the figures included (both pair and multibody).

Changing the number of structures: We also performed tests of the predictive ability of the fit by removing some structures from the fit. First, we removed three structures which were originally fit quite well: Z₂, Z₂, and L1₂ (NiAu₃). Removing these structures from the input set resulted in their energies changing by < 1 meV/atom. However, a much more critical test of the fit is to remove the structures which are fit most poorly: SQS14_a and SQS14_b. Removing these structures from the fit changes their energies by only 2–3 meV/atom. Thus, we are confident that the present k-space CE fit is both stable and predictive.

IV. RESULTS OF CURRENT CALCULATIONS

A. Mixing enthalpy: How good are previous calculations?

Using the k-space cluster expansion in combination with a mixed real/reciprocal space Monte Carlo code (canonical), one can obtain thermodynamic properties of NiAu alloys. Figure 5 shows the mixing enthalpy as a function of temperature, $H_{\text{mix}}(T)$. Monte Carlo calculations were performed for a $16^3 = 4096$ atom cell, with 100 Monte Carlo steps per site for averages. The simulation was started at an extremely high temperature, and slowly cooled down using a simulated annealing algorithm. Also shown in Fig. 5 is the value of the mixing energy of the completely random alloy. The difference between the Monte Carlo calculated $H_{\text{mix}}(T)$ and the random alloy energy is precisely the energetic effect of short-range order. We have fit the values of $H_{\text{mix}}(T)$ to linear and quadratic functions of $T = 1/k_B T$ to extrapolate the values down in temperature below the point at which coherent phase separation occurs in the simulation. (Both fits gave virtually identical results, so the linear fit is used here and below.) This allows us to ascertain the value of the mixing enthalpy at 1100 K, near the temperature where this quantity has been experimentally

measured. These results are tabulated in Table IV, which shows both the effects of atomic relaxation (~ 100 m eV/atom) and SRO (~ 25 m eV/atom) on the mixing enthalpy, and compares the value of atomically relaxed and short-range ordered mixing energy with those values from experiment. One can see that by taking into account both relaxation and SRO, LDA produces a value for the mixing energy which is only different from experiment by 15–20 m eV/atom. Thus, we conclude from this comparison that high quality LDA calculations provide accurate energetics for the NiAu system.

The preceding discussion leads to a number of conclusions regarding previous calculations of H_{mix} :

(i) Since relaxation reduces H_{mix} by ~ 100 m eV/atom, the unrelaxed H_{mix} values (listed in Table I) have to be reduced by this amount to appropriately compare with experiment.

(ii) Since SRO reduces H_{mix} by ~ 25 m eV/atom, the results of previous calculations that omitted SRO (all except (i) in Table I) have to be adjusted accordingly.

(iii) In light of the fact that the empirical potential-based and ASA-based methods (LMTO and ASW) were shown to be inaccurate with respect to full-potential LDA methods for unrelaxed, ordered compounds (Table II), the results of relaxed, mixing energies of random alloys appear to be questionable using these schemes.

B. Configurational or non-configurational entropy?

From the fit of the Monte Carlo data in Fig. 5, one can find the configurational entropy of the $\text{Ni}_{0.5}\text{Au}_{0.5}$ disordered phase by integrating the energy down from infinite temperature (where the configurational entropy is known):

$$S(T) = S(T = \infty) + E(T) = T \int_0^Z \frac{E(\epsilon)}{\epsilon} d\epsilon \quad (14)$$

The configurational entropy obtained from thermodynamic integration in this way is

$$S_{conf}(\text{Ni}_{0.5}\text{Au}_{0.5}; T = 1100\text{K}) = 0.56k_B; \quad (15)$$

compared to the "ideal" (infinite temperature) value of

$$S_{\text{conf}}(\text{Ni}_{0.5}\text{Au}_{0.5}; T = 1) = 0.69k_B; \quad (16)$$

This calculated value for the configurational entropy of mixing can be compared with the experimentally measured values of total entropy of mixing: Calorimetric measurements give $S(T = 1150\text{K}) = 1.04k_B$ [1] while EMF measurements give $S(T = 1173\text{K}) = 1.08k_B$ [11]. Thus, we can obtain an estimate of the non-configurational entropy, and find it to be large: $S_{\text{non-conf}}(T = 1100\text{K}) = 1.04 - 0.56 = 0.48k_B$. This non-configurational entropy is hence responsible for T_{MG} being so small experimentally, compared to all the theoretical results. In fact, if we use the calculated $H_{\text{mix}} = 93 \text{ meV/atom}$ and the combined \textit{experimental/calculated} $S_{\text{non-conf}} = 0.48k_B$ in the following formula:

$$T_{\text{MG}} = \frac{2 H_{\text{mix}}}{k_B + 2 S_{\text{non-conf}}} \quad (17)$$

we obtain $T_{\text{MG}} = 1100 \text{ K}$ and $k_B T_{\text{MG}} = H_{\text{mix}} = 1.02$, much closer to the experimental values ($T_{\text{MG}} = 1083 \text{ K}$ and $k_B T_{\text{MG}} = H_{\text{mix}} = 1.2$) than using the above formula neglecting non-configurational entropy ($T_{\text{MG}} = 2150 \text{ K}$ and $k_B T_{\text{MG}} = H_{\text{mix}} = 2.0$).

From this consideration of non-configurational effects, one should conclude that the accuracy of a calculation with configurational degrees of freedom only (as is done in most of the previous calculations [35]), should be determined by looking at the energetics, not the transition temperatures. Thus, previous calculations which give \textit{good} transition temperatures do so precisely because they have \textit{bad} energetics.

C. Short-range order of Ni_xAu_x solid solutions

Using the k -space CE and Monte Carlo, we may also compute the SRO of disordered Ni_xAu_x alloys. We show the results of our SRO simulations for $\text{Ni}_{0.4}\text{Au}_{0.6}$ in Fig. 6. For the SRO Monte Carlo calculations, a cell of $24^3 = 13824$ atoms was used, with 100 Monte Carlo steps for equilibration, with averages taken over the subsequent 500 steps. Several calculations and measurements of the SRO exist in the literature: Wu and Cohen [2] used diffuse x-ray scattering to deduce the atomic SRO of $\text{Ni}_{0.4}\text{Au}_{0.6}$ at $T = 1023 \text{ K}$. The measured

disorder intensity due to SRO must be separated from all the other contributions which give rise to disorder intensity, and for this purpose, Wu and Cohen used 25 real-space Fourier shells of SRO parameters, and found the rather surprising result that the peak intensity in reciprocal space due to SRO is of ordering-type and occurs at the point $k_{\text{SRO}} = (0.6, 0, 0)$, rather than $k_{\text{SRO}} = (0, 0, 0)$ which would be expected for a clustering alloy. Several authors have tried to account for this ordering nature of the SRO: Lu and Zunger [8] calculated the SRO (using 21 real-space shells) and found peaks at $(0.8, 0, 0)$ whereas Asta and Foiles [17] used an embedded atom method and found the SRO (using 8 real-space shells) to peak at $(0.5, 0, 0)$. Our calculations for the SRO of $\text{Ni}_{0.4}\text{Au}_{0.6}$ are given in Fig. 6. We have calculated the SRO at $T = 2300 \text{ K}$, above the miscibility gap temperature for our alloy Hamiltonian. We find that, using 8, 25, and 100 shells, the SRO peaks at $(0.65, 0, 0)$, $(0.40, 0, 0)$, and $(0.38, 0, 0)$ respectively, in good agreement with both the measurements of Wu and Cohen [$k_{\text{SRO}} = (0.6, 0, 0)$ for 25 shells] and also with previous calculations.

Equation (12) shows that the alloy Hamiltonian used in the Monte Carlo simulations is composed of three parts: the pair interaction terms, the many-body interaction terms, and the constituent strain terms. It is interesting to see the effect of each of these portions of the alloy Hamiltonian on SRO. Thus, in addition to the "full" calculations, which contain pairs, many-bodies, and constituent strain in the alloy Hamiltonian, we have also computed the SRO with (i) the CS energy only, and (ii) the CS energy plus the pair interactions. These results are shown in Fig. 7. (Because the CS energy is non-analytic in reciprocal space about the origin, many Fourier coefficients are required to converge the SRO of CS alone, thus we show only results using 100 shells of parameters in Fig. 7.) One can see that the SRO with CS only is dominated by almost constant streaks of intensity along the X line, and very little intensity elsewhere. This SRO pattern is understandable when one considers that the constituent strain at this composition (Fig. 2) is much softer (much lower in energy) in the (100) direction than along any other direction. Thus, (100)-type fluctuations in the random alloy are energetically favored, and because the constituent strain is dependent only on direction and not on the length of the wavevector, one should expect that all fluctuations

along the (100) will occur roughly equally, regardless of the length of the wavevector. This is precisely what we see in Fig. 7. Contrasting this SRO using CS only with that calculated both CS energy and pair interactions (but not multibody interactions) shows that the pair interactions create a peak in intensity along the X line, but significantly closer to than the peak intensity using the "full" alloy Hamiltonian. Thus, while the effect of pairs is to create a peak near the Γ point, the multibody interactions move this peak out from towards the X -point.

D. Standard inverse Monte Carlo would give unphysical interaction energies: a challenge

The statistical problem we have solved here involves the calculation of the alloy SRO at high temperature for given alloy Hamiltonian (fJ_{ij} , fJ_f , and E_{CS}). However, a popular technique used to study phase stability in alloys involves the "inverse" problem of determining a set of pair-only interactions fJ_{ij} from a measured or calculated SRO pattern, and the subsequent use of these pair interactions to determine thermodynamic properties other than the SRO. In fact, fJ_{ij} are often used to determine H_{mix} or phase stability. As we have mentioned in the introduction and described more fully in Ref. [36], inverting the SRO always removes information on energy terms that are SRO-independent, e.g., the volume deformation energy $G(x)$. This loss prevents, in principle, the interactions deduced from SRO from being applied to predict physical properties which depend on $G(x)$, such as H_{mix} . For example, in the case of NiAu, the SRO is of ordering-type. Thus, we expect that inverting the SRO of NiAu (e.g., via inverse Monte Carlo) would produce interactions fJ_{ij} which are of ordering-type, and using these interactions to predict the mixing enthalpy would result in the unphysical result $H_{mix} < 0$.

One might suspect that by changing the temperature, one could obtain a shift of the SRO from ordering- to clustering-type, and thus, the inverse technique would then produce interactions which would correctly give $H_{mix} > 0$. However, we have computed the SRO

for several temperatures, and find no evidence of a shift in SRO to clustering-type.

A test of our expectations by any of the practitioners of inverse Monte Carlo would certainly be welcomed. To that end, our SRO calculations are available for use as input to inverse Monte Carlo to extract interactions. These SRO calculations are available for a variety of compositions and temperatures, each with a large number of real-space SRO parameters. It would be of great interest to see whether the interactions extracted from inverting the SRO of NiAu would produce the correct sign of H_{mix} .

Acknowledgements

This work was supported by the Office of Energy Research (OER) Division of Materials Science of the Office of Basic Energy Sciences (BES), U.S. Department of Energy, under contract No. DE-AC36-83CH10093. The authors would like to thank Dr. M. Asta for providing the EAM values in Table II and Mr. D. Morgan for communicating his results to us prior to publication.

REFERENCES

- [1] Selected Values of Thermodynamic Properties of Metals and Alloys, R. R. Hultgren et al. eds. (Wiley, New York, 1963).
- [2] T. B. Wu and J. B. Cohen, *Acta Metall.* 31, 1929 (1983).
- [3] B. Golding and S. C. Moss, *Acta Metall.* 15, 1239 (1967).
- [4] B. Golding, S. C. Moss, and B. L. Averbach, *Phys. Rev.* 158, 637 (1967).
- [5] T. B. Wu, J. B. Cohen, and W. Yelon, *Acta Metall.* 30, 2065 (1982).
- [6] T. B. Wu and J. B. Cohen, *Acta Metall.* 32, 861 (1984).
- [7] H. E. Cook and D. de Fontaine, *Acta Metall.* 17, 915 (1969).
- [8] Z.-W. Lu and A. Zunger, *Phys. Rev. B* 50, 6626 (1994);
- [9] L. G. Ferreira, A. A. Mbaye, and A. Zunger, *Phys. Rev. B* 37, 10547 (1988).
- [10] See, e.g., V. Gerold and J. Kem, *Acta Metall.* 35, 393 (1987); W. Schweika and H.-G. Haubold, *Phys. Rev. B* 37, 9240 (1988); L. Reinhard, B. Schonfeld, G. Kosterz, and W. Buhner, *Phys. Rev. B* 44, 1727 (1990); L. Reinhard, J. L. Robertson, S. C. Moss, G. E. Ice, P. Zschack, and C. J. Sparks, *Phys. Rev. B* 45, 2662 (1992).
- [11] M. Bienzle, T. Oishi, and F. Sommer, *J. of Alloys and Compounds* 220, 182 (1995).
- [12] T. Deutsch and A. Pasturel, in *Stability of Materials*, edited by A. Gonis, P. Turchi, and J. Kudrnovsky, NATO-ASI Series (Plenum, 1996).
- [13] C. Amador and G. Bozzolo, *Phys. Rev. B* 49, 956 (1994).
- [14] C. Colinet, J. Eymery, A. Pasturel, A. T. Paxton, and M. van Schilfegaarde, *J. Phys.: Condens. Matter* 6, L47 (1994).
- [15] D. Morgan and D. de Fontaine (private communication).

- [16] S. Takizawa, K. Terakura, and T. Mohri, Phys. Rev. B 39, 5792 (1989).
- [17] M. Asta and S.M. Foiles, Phys. Rev. B 53, 2389 (1996).
- [18] R. Tetot and A. Finel, in Stability of Materials, edited by A. Gonis, P. Turchi, and J. Kudrnovsky, NATO ASI Series (Plenum, 1996).
- [19] J. Eymery, F. Lancon, and L. Billard, J. Phys. I France 3, 787 (1993).
- [20] J.W.D. Connolly and A.R. Williams, Phys. Rev. B 27, 5169 (1983).
- [21] D. de Fontaine, Solid State Phys. 34, 73 (1979).
- [22] A recent review is given in A. Zunger, in Statics and Dynamics of Alloy Phase Transformations, edited by P.E.A. Turchi and A. Gonis, NATO ASI Series (Plenum, New York, 1994) p. 361.
- [23] For a list of many cases in which ASA and full-potential formation energies significantly disagree, see Table I in C. Wolverton and A. Zunger, Phys. Rev. B 50, 10548 (1994).
- [24] D.M. Wood and A. Zunger, Phys. Rev. B 40, 4062 (1989).
- [25] A. Zunger, in Handbook of Crystal Growth, Vol. 3, D.T.J. Hurle, ed., (Elsevier, 1994).
- [26] J.E. Bernard and A. Zunger, Appl. Phys. Lett. 65, 165 (1994).
- [27] The Ni-Au system is especially difficult for the EAM. Similar comparisons between EAM and LDA for other systems (e.g., Cu-Ag) have yielded EAM results significantly closer to LDA. (M. Asta, private communication).
- [28] D. J. Singh, Planewaves, Pseudopotentials, and the LAPW Method, (Kluwer, Boston, 1994).
- [29] Generally, it was found that relaxing the cell-internal degrees of freedom provided much more energy lowering (by roughly a factor of 10) than the energy lowering of cell-external coordinates. For some low symmetry monoclinic structures relaxation of the length of

the unit cell vectors provided an insignificant amount of energy lowering, and thus the energy lowering associated with the variation of the angle of the unit cell vectors was neglected.

- [30] E. Wigner, Phys. Rev. **46**, 1002 (1934).
- [31] S. Froyen, Phys. Rev. B **39**, 3168 (1989)
- [32] A. Zunger, S.-H. Wei, L. G. Ferreira, and J. E. Bernard, Phys. Rev. Lett. **65**, 352 (1990).
- [33] D. B. Laks, L. G. Ferreira, S. Froyen, and A. Zunger, Phys. Rev. B **46**, 12587 (1992).
- [34] V. Ozolinš, C. Wolverton, and A. Zunger (to be published).
- [35] Some of the previous calculations (ϵ^0 , ϵ^i , ϵ^j of Table I) estimated the effects of vibrations on the phase diagram, either using a simple Debye model (ϵ^0) with LDA bulk modulus calculations or continuous-space Monte Carlo simulations (ϵ^i , ϵ^j) using the elastic response of an empirical potential.
- [36] C. Wolverton, A. Zunger, and B. Schonfeld, Solid State Commun. **101**, 519 (1997).

FIGURES

FIG .1. LAPW calculations of $q^{(1)}(a_2; \hat{k})$ of Eq. (2) for NiAu. Shown are (a) q^{Ni} and (b) q^{Au} for six principle directions.

FIG .2. LAPW calculations of $E_{CS}(\hat{k}; x)$ for NiAu for six principle directions.

FIG .3. (a) Pair and (b) multibody interaction energies for NiAu. The multibody figures are defined by the following lattice sites, in units of $a=2$ (the origin is contained in all figures): $J_3 = (110), (101)$, $K_3 = (110), (200)$, $N_3 = (200), (002)$, $P_3 = (110), (103)$, $Q_3 = (110), (220)$, $J_4 = (110), (101), (011)$, $K_4 = (110), (101), (200)$, and $L_4 = (110), (101), (211)$.

FIG .4. Cluster expansion fitting error in NiAu versus the number of pair interactions included in the fit.

FIG .5. $H(T)$ computed for $Ni_{0.5}Au_{0.5}$ from a combination of the k-space cluster expansion and Monte Carlo simulations.

FIG .6. Monte Carlo-calculated short-range order of $Ni_{0.4}Au_{0.6}$ in the $(hk0)$ plane using (a) 8, (b) 25, and (c) 100 shells of Warren Cowley SRO parameters. Peak intensity is red shaded contour while the lowest contours are shaded blue. Contours are separated by 0.1 Laue unit in each plot.

FIG .7. Monte Carlo-calculated short-range order of $Ni_{0.4}Au_{0.6}$ using (a) constituent strain terms only, (b) constituent strain and pair terms, and (c) constituent strain, pair, and multibody terms in the alloy Hamiltonian. Peak intensity is red shaded contour while the lowest contours are shaded blue. Contours are separated by 0.1 Laue unit in each plot.

TABLES

TABLE I. Summary of energy calculations performed for $\text{Ni}_{1-x}\text{Au}_x$ alloys. Shown are the methods used to compute $T=0$ energetics, as well as the type of cluster expansion (CE) and statistics used. Also given is the mixing energy of the $T \rightarrow 0$ random alloy near $x=1/2$, and the calculated miscibility gap temperature, if available. FLAPW = full-potential linearized augmented plane wave method, FLMT O = full-potential linear m u n-tin orbital method, ASW = augmented spherical wave method, LM TO -ASA = linear m u n-tin orbital method in the atomic sphere approximation, EAM = embedded atom method, MC = Monte Carlo, CVM = cluster variation method, MF = mean-field, SOE = second-order expansion.

Authors	Method			Results	
	T = 0 Energy	Cluster	Statistics	$H_{\text{mix}}^{\text{fcc}}$	$T_{\text{MG}} \text{ (K)}$
		Expansion Technique			
Wolverton and Zunger ^a	FLAPW	k-space CE	MC	+ 118	
Lu and Zunger ^b	FLAPW	G	MC	+ 127	
Deutsch and Pasturel ^c	FLMT O	G	none	+ 136	
Takizawa, Terakura, and Mohri ^d	ASW	CW	CVM	+ 170	
Amador and Bozzolo ^e	LM TO -ASA	CW	CVM	+ 150	
Colinet et al. ^f	LM TO -ASA	G	CVM	+ 67	1200-1400
Morgan and de Fontaine ^g	LM TO -ASA + "Elastic Springs"	G	CVM	+ 98	2330
Eymery et al. ^h	Empir. Potential	Simulation	none	+ 60	
Tetot and Finel ⁱ	Empir. Potential	Simulation	MC	+ 48 ^m	950
Deutsch and Pasturel ^c	Empir. Potential	Simulation	none	+ 83	
Asta and Foiles ^j	EAM	SOE	MC / MF	+ 78	2460
Expt. (Calorimetry) $T = 1150 \text{ K}$ ^k				+ 76	
Expt. (EMF) $T = 1173 \text{ K}$ ^l				+ 77	
Expt. (Phase Diagram)					1083

^aPresent results.

^bRef. [8]

^cRef. [12]

^dRef. [16]

^eRef. [13]

^fRef. [14]

^gRef. [15]

^hRef. [19]

ⁱRef. [18]

^jRef. [17]

^kRef. [1]

^lRef. [11]

^m at T = 1150 K

TABLE II. Comparison of formation enthalpies $H_f(\text{eV})$ for Ni-Au ordered compounds. Nomenclature for the ordered structures is the same as that used in Ref. [22]. All energies in meV/atom. Numbers in parentheses indicate unrelaxed energies.

Structure	Fully Relaxed	Partially Relaxed		Empirical			
	FLAPW ^a	FLAPW ^b	FLMTO ^c	ASW ^d	LMTO ^e	Potential ^c	EAM ^j
NiAu (L1 ₀)	+76.1 (+98.1)	+76.8	+79.4 (+96.4)	(+59)	(+116.6)	+57.9(+73.9)	+21.4(+91.1)
Ni ₂ Au ₂ (Z2)	+70.2 (+286.7)	+124.3	+123.1 (+300.1)		(+213.4)	+62.3(+127.7)	130.3(+208.6)
NiAu (L1 ₁)	+166.8 (+192.3)	+167.6	+175.4		(+177.9)		+72.9(+159.7)
NiAu (\40 ⁰⁰)	+84.8 (+93.5)	+83.8	+89.9		(+114.3)		1.9(+96.4)
Ni ₃ Au (L1 ₂)	+77.5	+75.5	+80.7	+42	+92.4	+58.1	+77.1
Ni ₃ Au (D0 ₂₂)	+75.0 (+75.0)		+81.5		(+95.3)		
NiAu ₃ (L1 ₂)	+78.9	+78.2	+78.0	+52	+89.4	+54.1	+86.1
NiAu ₃ (D0 ₂₂)	+68.6 (+68.7)		+68.0		(+76.4)		

^aPresent results. Complete atomic relaxation via quantum mechanical forces and total-energy minimization.

^bRef. [8]. Partial atomic relaxation via continuum elasticity, using Eqs. (2)–(6).

^cRef. [12]

^dRef. [16]

^eRef. [15]. LMTO-ASA with sphere radii chosen to minimize charge transfer.

^jRef. [17]

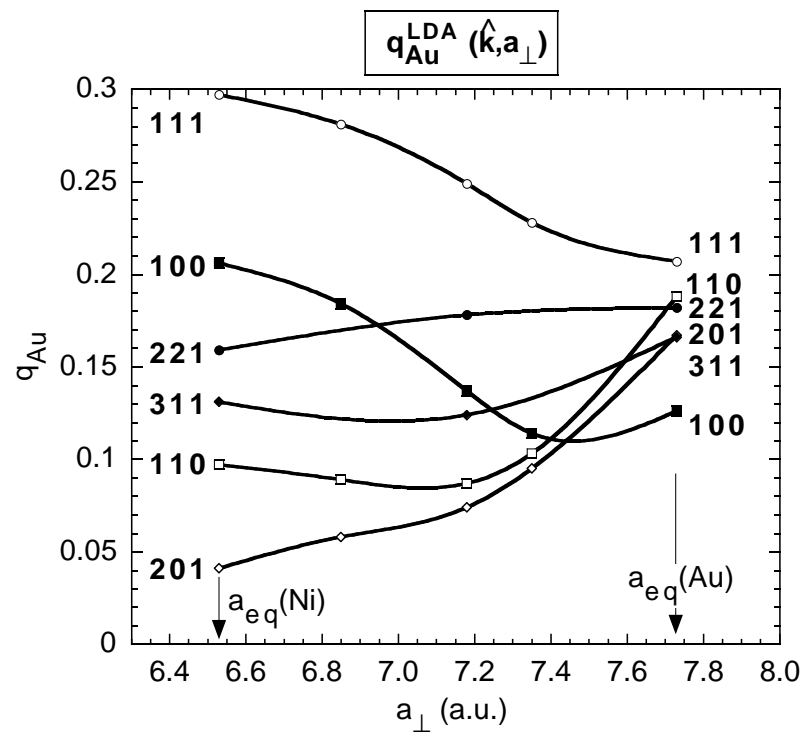
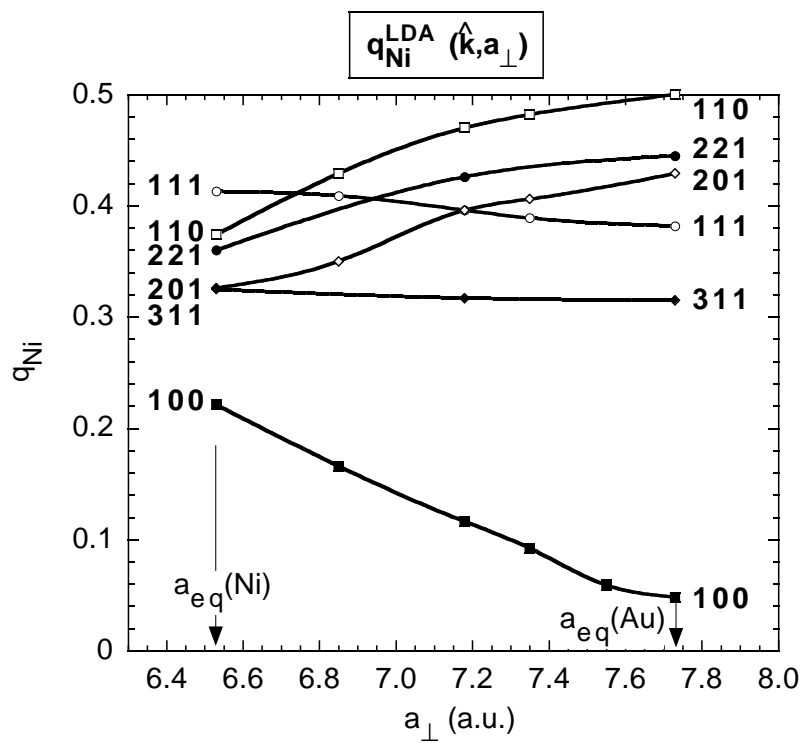
TABLE III. Listing of the LAPW calculated unrelaxed and relaxed $H(\hat{k})$ [in meV/atom] for Ni_xAu_{1-x} . Many of the structures calculated here can be characterized as a $(Ni)_p(Au)_q$ superlattice of orientation \hat{k} . We use the nomenclature of Ref. [22] for structure names.

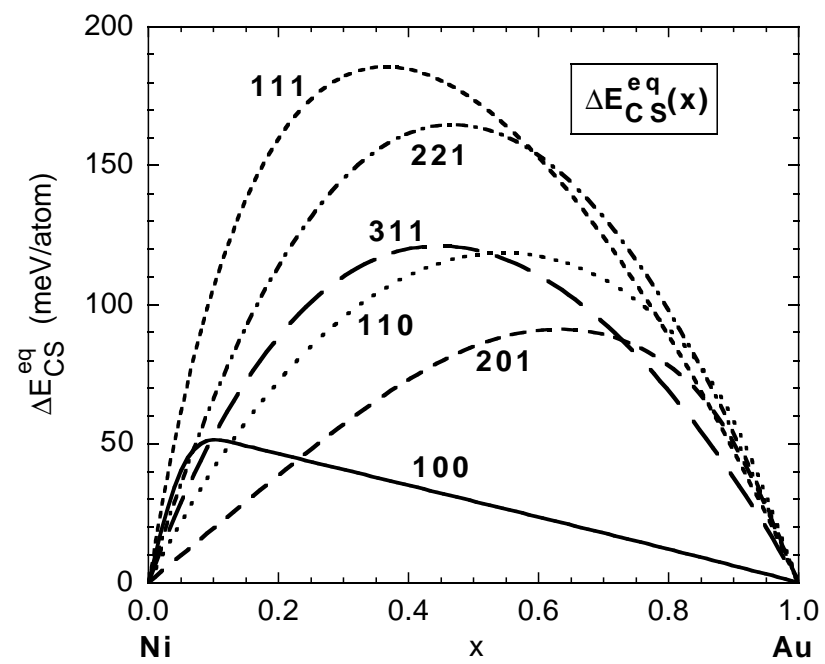
Orientation formula	[001]	[011]	[012]	[111]	[113]
AB	$L1_0$	$L1_0$	$L1_0$	$L1_1$	$L1_1$
Unrelaxed	+ 98.1	+ 98.1	+ 98.1	+ 192.3	+ 192.3
Relaxed	+ 76.1	+ 76.1	+ 76.1	+ 166.8	+ 166.8
CE (Relaxed)	+ 74.8	+ 74.8	+ 74.8	+ 167.1	+ 167.1
A_2B	1	1		1	
Unrelaxed	+ 207.8	+ 123.3		+ 288.5	
Relaxed	+ 105.7	+ 98.9		+ 202.2	
CE (Relaxed)	+ 105.9	+ 102.4		+ 208.4	
AB_2	2	2		2	
Unrelaxed	+ 151.7	+ 126.3		+ 200.9	
Relaxed	+ 38.3	+ 102.6		+ 100.9	
CE (Relaxed)	+ 37.8	+ 98.8		+ 94.5	
A_3B	Z1	Y1	DO_{22}	V1	W1
Unrelaxed	+ 221.7	+ 148.5	+ 75.0	+ 290.8	
Relaxed	+ 89.9	+ 99.2	+ 75.0	+ 193.7	+ 125.7
CE (Relaxed)	+ 94.3	+ 91.3	+ 69.1	+ 189.6	+ 120.8
AB_3	Z3	Y3	DO_{22}	V3	W3
Unrelaxed	+ 142.0	+ 104.1	+ 68.7	+ 172.8	
Relaxed	+ 32.4	+ 78.7	+ 68.6	+ 83.0	+ 88.4
CE (Relaxed)	+ 28.2	+ 77.7	+ 67.6	+ 79.1	+ 83.2
A_2B_2	Z2	Y2	$\sqrt{40}''$	V2	W2
Unrelaxed	+ 286.7	+ 192.3	+ 93.5	+ 335.8	+ 144.2
Relaxed	+ 70.2	+ 96.6	+ 84.8	+ 162.4	+ 93.6
CE (Relaxed)	+ 69.9	+ 101.1	+ 88.3	+ 166.7	+ 99.3
A_pB_p ($p \neq 1$)					
Unrelaxed	+ 576.2	+ 576.2	+ 576.2	+ 576.2	+ 576.2
Relaxed	+ 30.8	+ 117.7	+ 84.8	+ 173.8	+ 119.8
CE (Relaxed)	+ 30.8	+ 116.1	+ 86.8	+ 172.5	+ 117.9
Other Structures					
	$L1_2$ (A_3B)	$L1_2$ (AB_3)	$D7$ (A_7B)	$D7_b$ (A_7B)	
Unrelaxed	+ 77.5	+ 78.9	+ 82.9	56.8	
Relaxed	+ 77.5	+ 78.9	+ 82.9	56.8	
CE (Relaxed)	+ 80.7	+ 78.6	+ 98.5	57.6	
	SQS14a (A_6B_2)	SQS14b (A_2B_6)	Z6 ($A_3B_3 - 100$)	Z5 ($A_2B_3 - 100$)	
Unrelaxed	+ 183.2	+ 118.2	+ 355.5	+ 273.3	

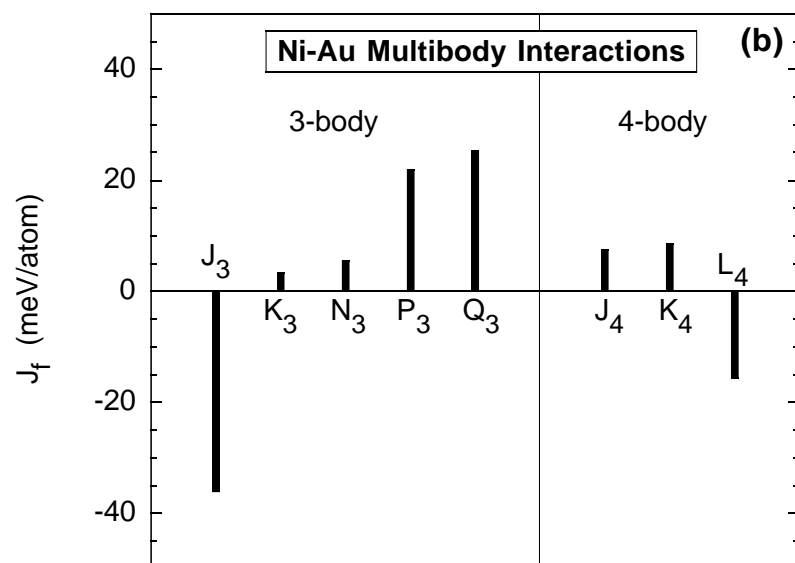
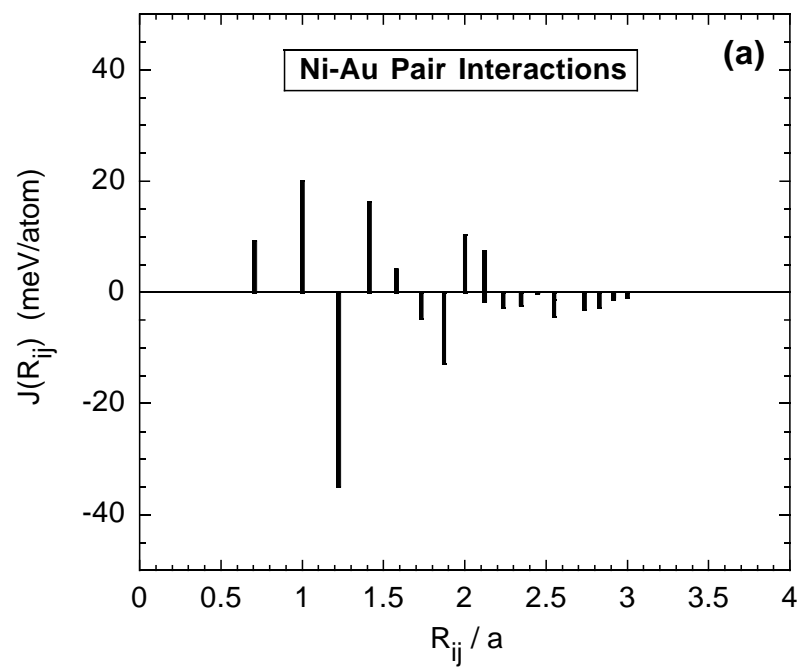
Relaxed	+ 96.8	+ 59.8	+ 63.2	+ 57.1
C E (Relaxed)	+ 81.5	+ 75.0	+ 62.5	+ 57.9

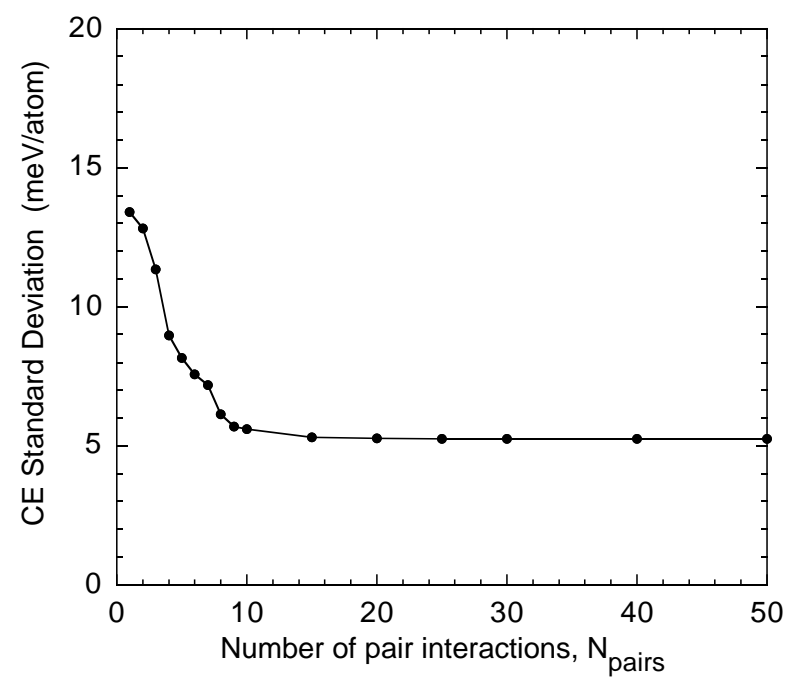
TABLE IV. H_{mix} for $\text{Ni}_{0.5}\text{Au}_{0.5}$. All energies in meV/atom. SQ S-4 refers to a 4-atom special quasi-random structure (Y2). This table shows the effects of relaxation (first line minus second line) and short-range order (third line minus fourth line) on the mixing energy.

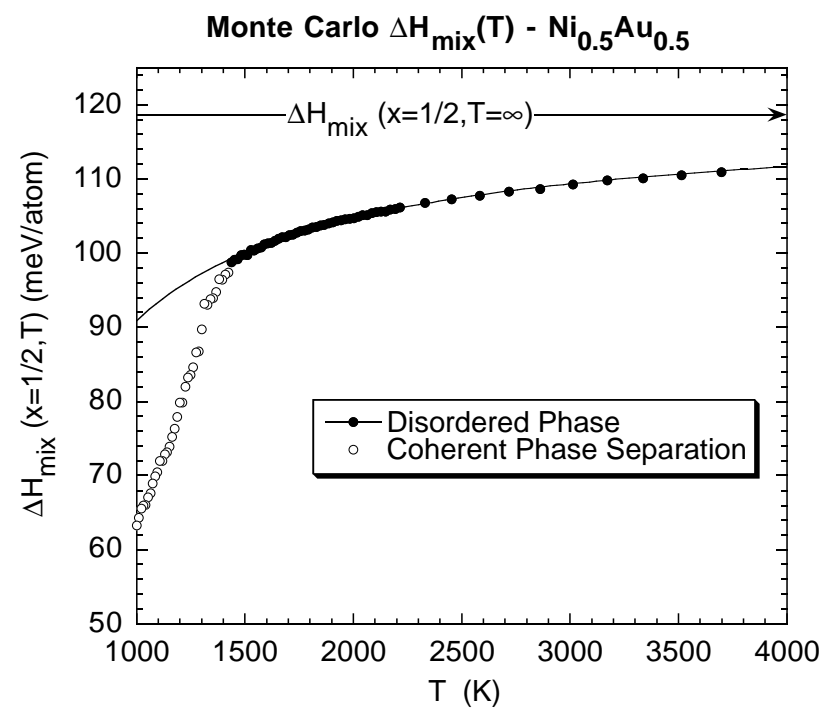
	H_{mix}
SQ S-4 Unrelaxed ($T = 1$)	+ 192
SQ S-4 Relaxed ($T = 1$)	+ 97
CE Relaxed ($T = 1$)	+ 118
CE Relaxed ($T = 1100\text{K}$)	+ 93
Expt. (Calorimetry) $T = 1150\text{ K}$	+ 76
Expt. (EMF) $T = 1175\text{ K}$	+ 77











This figure "fig6.gif" is available in "gif" format from:

<http://arxiv.org/ps/cond-mat/9701203v1>

This figure "fig7.gif" is available in "gif" format from:

<http://arxiv.org/ps/cond-mat/9701203v1>